



## Full Length Article

# Determination of the oxidation kinetics of high loaded CuO-based materials under suitable conditions for the Ca/Cu H<sub>2</sub> production process



L. Díez-Martín<sup>a,\*</sup>, G. Grasa<sup>a</sup>, R. Murillo<sup>a</sup>, M. Martini<sup>b</sup>, F. Gallucci<sup>b</sup>, M. van Sint Annaland<sup>b</sup>

<sup>a</sup> Instituto de Carboquímica, ICB-CSIC, Miguel Luesma Castán 4, 50018 Zaragoza, Spain

<sup>b</sup> Eindhoven University of Technology, P.O. Box 513, 5600 MB Eindhoven, The Netherlands

## ARTICLE INFO

## Keywords:

Ca/Cu looping process  
CuO-based materials  
Cu oxidation kinetics  
Pressure effect

## ABSTRACT

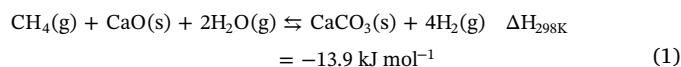
In this work, the oxidation reaction of high loaded CuO-based materials was investigated under atmospheric and pressurized conditions. The oxygen transport capacity of the materials was firstly tested in the TGA and no losses greater than 5% were observed along 100 oxidation/reduction cycles. The kinetic parameters governing the oxidation reactions of the selected CuO-based materials were determined using a shrinking core model with chemical reaction control. The experimental results suggested that a SCM with chemical reaction control is able to predict the oxidation conversion of high loaded CuO-based materials in powder and pellet form. On the other hand, the effect of total pressure on materials reactivity was analyzed. The kinetic parameters obtained under atmospheric conditions were applied to fit the experimental data obtained under pressurized conditions. The results confirmed that the pressure has not an important effect on the oxidation kinetics of high loaded CuO-based materials and the parameters obtained at atmospheric pressure can be applied to study the oxidation under pressurized conditions.

## 1. Introduction

It is nowadays generally accepted that a reduction of anthropogenic greenhouse gas emissions is necessary in a short period of time to limit the human influence on the climate change. CO<sub>2</sub> capture and sequestration has been accepted as an appropriate strategy to decrease emissions of greenhouse gases from combustion processes. However, the increase of capital cost and the decrease in the net power efficiency (efficiency penalty) of the plant using conventional gas separation techniques is a drawback for these processes [1]. Therefore, the implementation of new CO<sub>2</sub> capture technologies to mitigate CO<sub>2</sub> emissions of power and chemical processes, is currently required. On the other hand, hydrogen is nowadays mainly used in ammonia, methanol and oil refining production plants and the demand of this chemical is expected to grow in a near future. Steam Methane Reforming (SMR) is the most widely used technology to produce H<sub>2</sub> at commercial scale with around 50% of the H<sub>2</sub> worldwide [2,3]. This process generates relevant CO<sub>2</sub> emissions (8.9–9.1 kgCO<sub>2</sub> kgH<sub>2</sub><sup>−1</sup>) [3]. Modern H<sub>2</sub> production plants use a SMR stepped process where the reforming reactor is followed by a High Temperature Shift (HTS) to maximize CO conversion and H<sub>2</sub> production [4,5] and, finally, a pressure swing adsorption (PSA) system to reach H<sub>2</sub> yields greater than 95%vol [6]. The expected increase of the worldwide H<sub>2</sub> demand makes it interesting to

develop and apply new CO<sub>2</sub> capture technologies to hydrogen production plants. These new capture technologies should always minimize the costs and the energy penalty compared with the commercially available capture technologies [7].

One of these new processes is the sorption enhanced steam methane reforming (SER) in which H<sub>2</sub> production is combined with inherent CO<sub>2</sub> capture in the same system. In the SER process a reforming catalyst is combined with a CO<sub>2</sub> sorbent in order to *in situ* remove the CO<sub>2</sub> as it is generated (Eq. (1)). The overall process is slightly exothermic and the addition of the CO<sub>2</sub> sorbent shifts the equilibrium to the right side (Le Chatelier's principle) of the reaction and, therefore, practically complete CH<sub>4</sub> and CO conversion can be achieved at lower temperatures. The traditional SER process usually operates at atmospheric pressure. This fact means that higher H<sub>2</sub> yield under relatively mild conditions of pressure and temperature can be produced.



The advantages of the SER process are numerous as it has been stated by several authors [8–15]. However, the sorbent regeneration by calcination of CaCO<sub>3</sub> to CaO is also needed to cyclically operate the process. By contrast, the calcination is a very endothermic reaction and, therefore, an additional source of energy must be supplied. One of the

\* Corresponding author.

E-mail address: [ldiezmartin@icb.csic.es](mailto:ldiezmartin@icb.csic.es) (L. Díez-Martín).

**Nomenclature**

T	temperature (K)
P	pressure (bar)
X <sub>ox</sub>	oxidation conversion (–)
m <sub>ox</sub>	mass of the fully oxidized material (mg)
m <sub>red</sub>	mass of the fully reduced material (mg)
m(t)	mass of the material at an specific time (mg)
OTC	oxygen transport capacity (mg O mg oxidized material <sup>–1</sup> )
%wt Cu	percentage of Cu content in the material (mg Cu/mg material)
t	time (s)
N <sub>A</sub>	number of moles of the specie A (moles O <sub>2</sub> )
S <sub>ext</sub>	surface area (m <sup>2</sup> )
L	particle or pellet radius (m)
b	stoichiometric coefficient of the Cu oxidation reaction (–)
k <sub>s</sub>	reaction rate constant (mol <sup>1–n</sup> m <sup>3n–2</sup> s <sup>–1</sup> bar <sup>d</sup> )
C <sub>g</sub>	gas concentration (mol m <sup>–3</sup> )
n	reaction order
k <sub>o</sub>	pre-exponential factor (mol <sup>1–n</sup> m <sup>3n–2</sup> s <sup>–1</sup> bar <sup>d</sup> )
R	universal gas constant (J mol <sup>–1</sup> K <sup>–1</sup> )
E <sub>a</sub>	activation energy (J mol <sup>–1</sup> )
r <sub>c</sub>	radius of unreacted core or reaction front (m)
h <sub>m</sub>	gas film mass transfer coefficient (m s <sup>–1</sup> )
D <sub>e</sub>	effective mass diffusivity (m <sup>2</sup> s <sup>–1</sup> )
D <sub>pore</sub>	mass diffusivity inside mesopores (m <sup>2</sup> s <sup>–1</sup> )
D <sub>i</sub>	mass diffusivity (m <sup>2</sup> s <sup>–1</sup> )
D <sub>Kn</sub>	Knudsen diffusivity (m <sup>2</sup> s <sup>–1</sup> )
d <sub>pore</sub>	pore diameter (m)

M <sub>i</sub>	molecular weight of the specie i (g mol <sup>–1</sup> )
ΔH	reaction enthalpy (kJ mol <sup>–1</sup> )
S <sub>BET</sub>	specific surface area (m <sup>2</sup> g <sup>–1</sup> )
d	diameter of the pellet (m)
h	height of the pellet (m)

**Acronyms**

SMR	steam methane reforming
HTS	high temperature shift
PSA	pressure swing adsorption
ASU	air separation unit
CLC	chemical looping combustion
CLR	chemical looping reforming
CLOU	chemical looping with oxygen uncoupling
SER	sorption enhanced reforming
SCM	shrinking core model
CGSM	changing grain size model
TGA	thermogravimetric analyzer
HPMSB	high pressure magnetic suspension balance

**Greek letters**

τ	time required for complete conversion (s)
ρ	density of the material (kg m <sup>–3</sup> )
ρ <sub>b</sub>	molar density of the CuO in the particle (mol <sub>CuO</sub> m <sup>–3</sup> )
τ <sub>pore</sub>	tortuosity of the pores (–)
ε	porosity (–)
v	diffusion volume for the specific component (m <sup>3</sup> mol <sup>–1</sup> )

possible options consists on burning additional fuel under oxyfiring conditions to produce a gas stream with a high CO<sub>2</sub> concentration. In the recent years, an innovative process that aims at producing pressurized H<sub>2</sub> with reduced CO<sub>2</sub> emissions, commonly known as Ca/Cu looping process, has been proposed [16,17]. This innovative process has two main advantages with respect to the traditional SER process: in the first place, a pressurized gas stream is produced and no downstream compression is needed; secondly, an additional air separation unit (ASU) is not required to calcine the sorbent while generating a gas stream with high CO<sub>2</sub> concentration. High carbon capture rates can be achieved with this process [18,19]. Based on a patent by Abanades and Murillo [20], this process incorporates a second chemical loop, Cu/CuO, to the CaO/CaCO<sub>3</sub> loop in the SER process to solve the energy requirement during the sorbent regeneration stage. In this way, the exothermic reduction of CuO with H<sub>2</sub>, CO or CH<sub>4</sub> provides the energy to drive the calcination of CaCO<sub>3</sub>. The coupling of both endothermic and exothermic reactions in one single stage allows for higher integration as the heat is directly transferred without the need for intermediate heat exchange equipments. The basic Ca/Cu looping process consists of a sequence of three main reaction steps, which are adiabatically carried out in fixed-bed reactors operating in parallel. Fig. 1 shows the three main steps of the process that have to be accomplished in the presence of a CaO-based sorbent, a CuO-based material and a reforming catalyst. In the first stage of the process (A) the sorption enhanced steam reforming of methane to produce H<sub>2</sub> with inherent CO<sub>2</sub> capture (20 bar, 923 K) takes place. During a second step (B), the oxidation of the Cu material happens (20 bar, 1103 K). Finally, the calcination of CaCO<sub>3</sub> and simultaneous reduction of CuO is carried out in the step C (1 bar, < 1173 K). In a recent work, the H<sub>2</sub> production stage of the Ca/Cu process was validated under relevant experimental conditions [21]. In this research a gas stream containing 95%vol H<sub>2</sub> was obtained at 923 K using a space velocity of 2.5 kg CH<sub>4</sub> h<sup>–1</sup> kg cat<sup>–1</sup>, high enough to allow the process scaling up. Fernández et al. [22] have studied the step B of the process applying a dynamic model to describe the Cu oxidation

reaction in a fixed bed facility. They found that a pressure of 20 bar could be reasonable to minimize the calcination of the sorbent during this step. The maximum temperature during Cu oxidation must be kept below 1173 K to minimize the calcination of CaCO<sub>3</sub> and the temperature profiles can be moderated by decreasing the concentration of the oxygen in the feed and the temperature of the inlet gas. Finally, the step C of the process has been evaluated in an adiabatic fixed bed using a dynamic pseudo-homogeneous model [23] and has been experimentally validated under industrially relevant conditions for this technology [24]. A sensitivity analysis of the main parameters involved in the process confirmed the viability of this step and an optimal CuO/CaCO<sub>3</sub> ratio ensured a suitable bed performance allowing that the calcination and reduction fronts advance together at moderate temperatures (1173 K) and leaving behind fully conversion of the materials.

The Ca/Cu looping process requires materials with suitable proportions of Ca and Cu that allows running the process cyclically. Cu-loads in the range of 65%wt have been proposed during the conceptual design of the Ca/Cu process [17]. Several synthesis routes have been

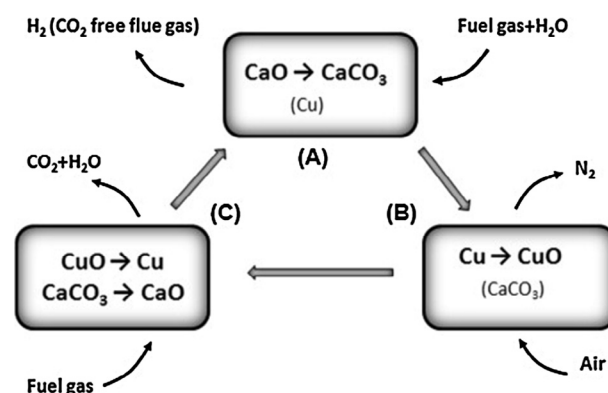


Fig. 1. General scheme of the Ca/Cu looping process.

reported in the literature to synthesize CuO-based materials suitable for different applications as Chemical Looping Combustion (CLC), Chemical Looping with Oxygen Uncoupling (CLOU), Chemical Looping Reforming (CLR) and Ca/Cu processes as for example co-precipitation, mechanical mixing, spray-drying, impregnation, deposition-precipitation or freeze granulation have been followed by different authors [25–35]. The assessment of reactivity and chemical stability of these materials is essential for the development of these processes. Although very important for the design of Ca-Cu loops, an extensive work specifically dealing with the oxidation kinetics of CuO-based materials is still lacking in the literature. Up to now, different gas-solid models such as the shrinking core model (SCM) [26,29,36–41], the changing grains size model (CGSM) [39,42,43] and the nucleation models [44,45] have been reported in the literature to determine the kinetic parameters of oxidation reactions of different metal oxide materials. Regarding to the oxidation reaction, García-Labiano et al. [26], applied the SCM to determine the kinetic behavior of a 10%wt CuO/Al<sub>2</sub>O<sub>3</sub> material prepared by impregnation and they obtained a low dependence of the reaction rates with temperature with activation energy values varying from 7 kJ mol<sup>-1</sup> to 15 kJ mol<sup>-1</sup> and reaction order approaching 1. In the same way, Maya et al. [39] tested the oxidation action of CuO-particles using a CGSM (Cu loads between 8 and 20%wt) and they found activation energy values for oxidation from 11 kJ mol<sup>-1</sup> to 16 kJ mol<sup>-1</sup>, with reaction orders from 0.8 to 0.9.

Within the Ca/Cu process, the oxidation reaction (step B, in Fig. 1) takes place at temperatures below 1123 K and at elevated pressures to minimize the loss of CO<sub>2</sub> caused by the partial calcination of CaCO<sub>3</sub> [17]. A few number of authors analyzed the effect of pressure in the reduction and oxidation reactions of copper-based materials [42,46]. Abad et al. [42] studied the effect of pressure on the behavior of a copper-based oxygen carrier with 10%wt of CuO using the CGSM. They found that an increase in total pressure had a negative effect on the reaction rates of the oxygen carriers. In the same way, Hamers et al. [42,46] analyzed the effect of pressure on the kinetics of reduction and oxidation of particles with similar CuO content (13%wt) and they also found a decrease in the reactivity of the particles at higher pressures. However, San Pio et al. [47] have recently published their results on the reduction kinetics of 12.5%wt CuO/Al<sub>2</sub>O<sub>3</sub> particles and no negative effect of pressure on the reactivity of the materials has been found. They concluded that the negative effect that has been observed by some authors could be caused by external mass transfer limitations rather than physical effects of the pressure on the reactivity. Therefore, contradictory results have been reported for materials with low CuO contents and therefore the analysis of the influence of pressure in the reactivity of high loaded CuO-based materials is needed.

As it has been mentioned in previous paragraphs the Ca/Cu looping process requires highly stable CuO-based materials which can suitably be adapted to different oxidation and reduction conditions, temperatures and pressures. The present work is focused on determining the kinetic parameters for the oxidation reaction of two different materials with high Cu loads (65% wt). The effect of reaction temperature, O<sub>2</sub> partial pressure and total operation pressure on reaction rate were evaluated. The kinetic parameters determined were included in a particle reaction model that served to describe the experimentally observed oxidation conversion of Cu-based pellets.

## 2. Experimental

### 2.1. Materials

Two highly loaded CuO-based materials, one of them synthesized by Johnson Matthey PLC (Cu65Al\_COP) and the other by ICB-CSIC (Cu65MgAl\_COP) with Cu loads around 65%wt and supported on Al<sub>2</sub>O<sub>3</sub> and MgAl<sub>2</sub>O<sub>4</sub> respectively, were evaluated in this work. The materials, synthesized by a co-precipitation technique, were tested in powder (< 100 μm) and in pellet. The co-precipitation route is described as

follows: nitrate solutions (chemical reagent purity ≥ 99%) containing Cu or Al or Mg, respectively, were prepared and the pH of the solutions was adjusted adding Na<sub>2</sub>CO<sub>3</sub>. The resulting solution was stirred and filtered. The precipitate formed was washed several times with distilled water to remove excess nitrate and alkali ions. Then, the solid was dried and finally calcined. In addition, pellets with cylindrical shape (with a pellet height = pellet diameter) of these materials were also prepared. These materials were also characterized by different techniques. The elementary composition of fresh materials was determined by ICP-OES. The device used in this analysis was a Spectroblue apparatus of Ametek. The presence of crystalline species in fresh and cycled samples was identified by X-ray diffraction (XRD) by an X-ray diffractometer Bruker AXS D8ADVANCE that employs CuKα radiation. The fresh materials were characterized by TPR analysis to study the main temperatures of reducible species present in each CuO-based material. The analysis was carried out in a PulseChemisorb 700 supplied by Micromeritics. The technique of N<sub>2</sub> physisorption applying the BET method was used to calculate the specific surface area in an Micromeritics ASAP 2020 apparatus. The solid density was determined by He pycnometry in a Micromeritics ACCUPYC II device and the porosity of the samples was determined using Hg porosimetry with a POREMASTER of Quantachrome apparatus. The main physical and chemical properties of these solids are shown in Table 1.

### 2.2. Apparatus

Two different thermobalances were used during this research to work either under atmospheric or pressurized conditions. The purity of the reactant gases used in the experiments was higher than 99.99%.

A thermogravimetric analyzer (TGA-CI Electronics Ltd.) was used to determine the chemical stability and the kinetics of the oxidation reaction at atmospheric pressure (Fig. 2a). This equipment consisted of two concentric quartz tubes located inside a furnace. Each sample was introduced in a platinum pan placed at the bottom of this device. The TGA allows the weight change of a sample to be measured in terms of time for a controlled atmosphere of reacting gas and temperature.

A high pressure magnetic suspension balance (HPMSB – Rubotherm) was used to study the oxidation reaction at different pressures (Fig. 2b). This device can operate between 473 K and 1473 K and 1 bar to 30 bars. The CuO-based sample is placed in a porous quartz glass sample holder. The basket is hanging on an Ir wire that is connected to a permanent magnet and the mass is determined by the

**Table 1**

Main physical and chemical properties of the co-precipitated materials tested in this work.

Powdered materials	Cu65Al_COP	Cu65MgAl_COP
Support material	Al <sub>2</sub> O <sub>3</sub>	MgAl <sub>2</sub> O <sub>4</sub>
wt% Cu	65.5 ± 6.23 × 10 <sup>-2</sup>	65.0 ± 5.17 × 10 <sup>-2</sup>
OTC (mgO mg material <sup>-1</sup> )	0.164 ± 2.41 × 10 <sup>-4</sup>	0.163 ± 1.57 × 10 <sup>-4</sup>
Particle diameter (μm)	75	60.5
% ε (oxidized)	60	75
ρ (kg m <sup>-3</sup> )	5585	5510
ρ <sub>b</sub> (molCuO m <sup>-3</sup> )	55,407	56,050
S <sub>BET</sub> (m <sup>2</sup> g <sup>-1</sup> ) – oxidized	21	19
PELLETS	P_Cu65Al_COP	P_Cu65MgAl_COP
wt% Cu	60.1 ± 5.53 × 10 <sup>-2</sup>	64.8 ± 4.89 × 10 <sup>-2</sup>
OTC (mgO mg material <sup>-1</sup> )	0.149 ± 1.35 × 10 <sup>-4</sup>	0.163 ± 1.22 × 10 <sup>-4</sup>
d (m)	3.3 × 10 <sup>-3</sup>	3 × 10 <sup>-3</sup>
h (m)	3.3 × 10 <sup>-3</sup>	3 × 10 <sup>-3</sup>
weight oxidized (kg)	65.6 × 10 <sup>-6</sup>	48 × 10 <sup>-6</sup>
ρ (kg m <sup>-3</sup> )	2300	2263
ρ <sub>b</sub> (molCuO m <sup>-3</sup> )	21,186	22,910
d <sub>pore</sub> (nm)	22	50
% ε (reduced pellet)	53	51
% ε (oxidized pellet)	48	43
S <sub>BET</sub> (m <sup>2</sup> g <sup>-1</sup> ) – reduced pellet	18	18
S <sub>BET</sub> (m <sup>2</sup> g <sup>-1</sup> ) - oxidized pellet	24	20

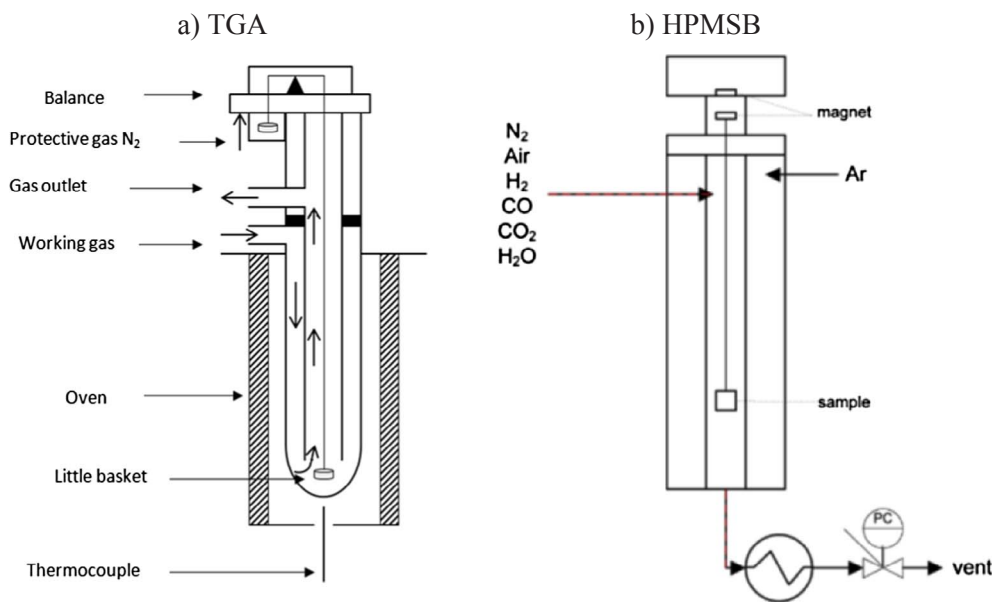


Fig. 2. a) Thermogravimetric analyzer, (TGA at ICB-CSIC), b) high pressure magnetic suspension balance (HPMSB at TU/e) used in this work.

changing magnet strength.

### 2.3. Experimental procedure

#### 2.3.1. Chemical stability

To test the chemical stability of the solids at atmospheric pressure, 100 reduction/oxidation cycles under isothermal conditions at 1123 K were carried out in the TGA apparatus described in the previous section. 15 mg of sample or 1 individual pellet were introduced respectively in a platinum pan suspended in the TGA apparatus in each test. A constant total flow of 280 ml min<sup>-1</sup> of gas was fed in at the top of the reactor, after being preheated by flowing through the external reactor tube along the furnace with a space velocity of 0.012 m s<sup>-1</sup> (this avoids external mass transfer limitations as described below). Reaction temperature and gas composition were constant in each test. Reduction and oxidation cycles were performed by a gas stream with 20 vol% H<sub>2</sub> in N<sub>2</sub> and 20 vol% O<sub>2</sub> in N<sub>2</sub> respectively, using a N<sub>2</sub> purge between each reduction and oxidation stage. A constant N<sub>2</sub> flow passed through the head of the thermobalance to prevent accumulation of reactive species on it. The Cu content in each material was calculated from the amount of oxygen reacting during successive reduction/oxidation cycles in the TGA. The conversion of CuO-based materials during the oxidation reaction has been calculated using the TGA apparatus through the mass change in the solid under different experimental conditions. The oxidation conversion was calculated using Equation (2), where  $m$  is the current mass and  $m_{ox}$  is the mass of the fully oxidized CuO-based material. In the same way, in order to analyze the chemical and mechanical stability of the materials, the oxygen transport capacity was

determined by Eq. (3) along multiple reduction-oxidation cycles. In this case,  $m_{red}$  represents the mass of the fully reduced form of the material.

$$X_{ox} = \frac{m(t) - m_{ox}}{m_{ox} - m_{red}} \quad (2)$$

where the oxygen transport capacity is defined as:

$$OTC = \frac{(m_{ox} - m_{red})}{m_{ox}} \quad (3)$$

#### 2.3.2. Kinetic tests

Oxidation tests at atmospheric pressure were carried out in order to determine the kinetic parameters for each material. This study was complemented by the analysis of the effect of total operating pressure on the oxidation kinetics of the materials. Preliminary tests were performed to assess the amount of sample required to avoid any mass transfer limitation due to sample mass and sample pan geometry, as well to determine the total gas flow that eliminated any gas film resistance. Around 10 mg of sample in powder form, or 1 individual pellet were loaded in the atmospheric TGA (Fig. 2a) in every test. The oxidation tests at atmospheric conditions were carried out using a total flow of 280 ml min<sup>-1</sup> in streams containing diluted O<sub>2</sub> in N<sub>2</sub>, at a space velocity of 0.012 m s<sup>-1</sup>. The effect of temperature (from 973 K to 1143 K) and reacting gas partial pressure (from 2.5 vol% O<sub>2</sub> until 40 vol% O<sub>2</sub>) were assessed. To determine the reaction order, consecutive oxidation/reduction cycles were performed at a constant temperature of 1123 K and varying the O<sub>2</sub> partial pressure. To determine the pre-exponential factor and activation energy tests were made through

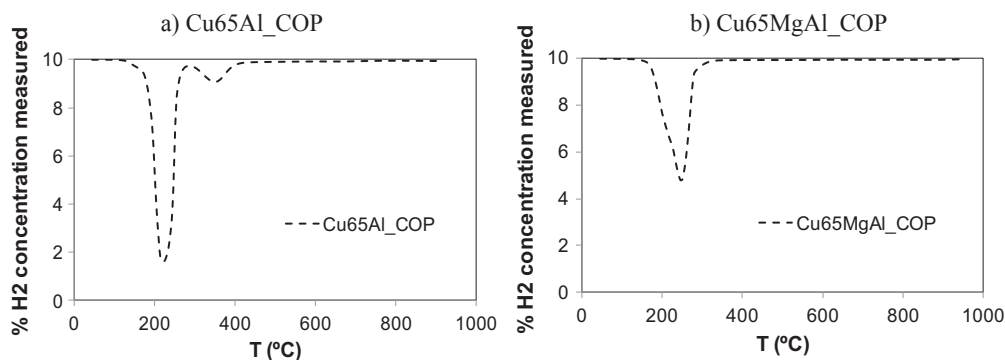


Fig. 3. Thermal programmed reduction tests at 10% vol H<sub>2</sub> of the Cu65Al\_COP and Cu65MgAl\_COP materials.



consecutive oxidation/reduction cycles varying temperature with a constant flow of 10 vol%  $O_2$  for powders and 20 vol%  $O_2$  for pellets. Each cycle included a reduction stage at the set temperature and gas composition (20 vol%  $H_2$  in  $N_2$ ) and 1 min of inert  $N_2$  purge.

To determine the effect of total pressure, the HPMSB was used (Fig. 2b). In each test, one single pellet was loaded in the pan with a total flow of  $480 \text{ ml min}^{-1}$  of gas in the apparatus. In this case, mixtures of air and  $N_2$  at different  $O_2$  concentrations were used to study the oxidation reaction at a space velocity of  $0.019 \text{ m s}^{-1}$ . The effect of temperature (from 973 K to 1143 K), reacting gas partial pressure (from 2.5 vol%  $O_2$  until 40 vol%  $O_2$ ) and pressure (1 bar – 20 bar) were analyzed in these experiments.

In addition, the step B of the Ca/Cu process was also simulated in the HPMSB considering several gas compositions and total pressures that could be expected during the operation of this step in the Ca/Cu looping process [17,22]. A constant oxygen composition during the test of 5 vol%  $O_2$  in  $N_2$  at 1123 K and 10 bar has been considered in one case, and 3 vol%  $O_2$  in  $N_2$  at 1123 K and 20 bar has been considered in other case. The kinetic parameters previously determined were applied to fit the experimental results obtained under these conditions.

### 3. Results and discussion

#### 3.1. Characterization and chemical stability

Fig. 3 shows the results from the TPR analysis for the materials on  $Al_2O_3$  (Fig. 3, a) and  $MgAl_2O_4$  (Fig. 3, b). The materials supported onto  $Al_2O_3$  present 2 differentiated  $H_2$  consumption peaks associated with the reduction of two different copper species. The main consumption peak (around 548 K) is related to the reduction of a well dispersed CuO and the second minor peak at temperatures close to 673 K is attributed to the presence of  $CuAl_2O_4$  in the materials. By contrast, in the case of materials supported onto  $MgAl_2O_4$ , there is only one reduction peak in the range 523 K–623 K, associated with CuO reduction. Although the CuO peaks of the materials showed different shapes, which is attributed to some kind of interaction between the active phase and the support, the total consumption of  $H_2$  (determined with the integration of the area above the curve of the % $H_2$  concentration measured versus time) was very similar for both materials with the same Cu load into the different supports.

The X-ray diffractograms of fresh and cycled samples of both types of materials are compiled in Fig. 4. The TPR results were corroborated by this analysis. The XRD of the materials supported onto  $Al_2O_3$  revealed the presence of CuO as well as  $CuAl_2O_4$ . The presence of this intermediate in CuO-based materials was also reported by other authors [27,32,48]. However, the ratio of intensity for the CuO and  $CuAl_2O_4$  peaks in the fresh and cycled samples remained constant, which means that the proportion of species is stable along cycling. On the other hand, no interaction between the active CuO and  $MgAl_2O_4$  was observed in the other kind of materials. The presence of alumina or magnesia was not detected in the case of  $MgAl_2O_4$  materials, indicating that all the  $Al_2O_3$  and MgO formed  $MgAl_2O_4$  or existed in amorphous phases.

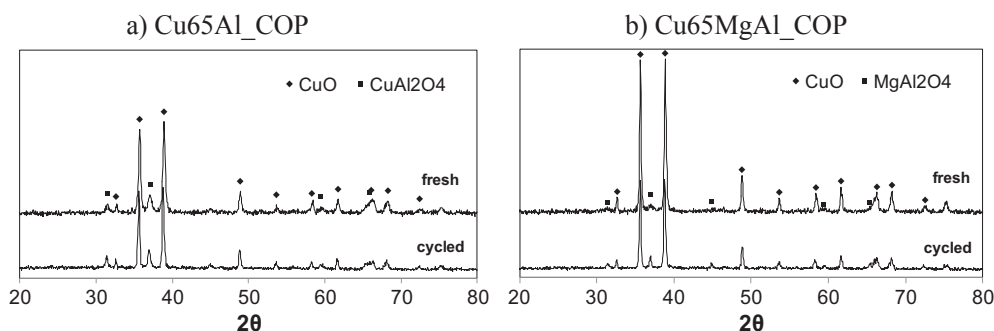


Fig. 4. X-ray diffractograms of the Cu65Al\_COP and Cu65MgAl\_COP materials.

Taking into account the results for the CuO-based materials that appear in literature [26–28,30–33,49] it seems that although in the majority of the cases the solids showed high redox reaction rate, contradictory results have been reported with respect to the mechanical and chemical stability of materials depending on the synthesis procedure. Arjmand et al. [27] tested CuO-based materials prepared by freeze granulation with  $Al_2O_3$  as support (40%wt of CuO) and they found that part of the active phase (either CuO or  $CuAl_2O_4$ ) is bound as  $CuAlO_2$  during incomplete reduction with slow kinetics for re-oxidation. On the other hand, García-Labiano et al. [26] tested materials with 10%wt of CuO for CLC applications demonstrated the feasibility of this oxygen carrier. Gayán et al. [30] tested the behavior of oxygen carriers with CuO contents around 15%wt in a CLC continuous unit of 500  $W_{th}$  during long-term tests getting high reactivity and mechanical durability of the materials without agglomeration. However, in spite of the good characteristics obtained with these materials, this kind of solids are not suitable for the Ca/Cu looping process because materials with higher Cu content to achieve the energy requirements of the sorbent calcination are needed. Imtiaz et al. [32] synthesized materials with higher CuO contents (between 70%wt to 87%wt of CuO) onto  $Al_2O_3$ . However, these solids were tested for a short number of reaction cycles and the OTC of the materials supported onto  $Al_2O_3$  was substantially below than the theoretical values due to the formation of intermediate species ( $CuAl_2O_4$  and  $CuAlO_2$ ) and the decomposition of  $CuAl_2O_4$ .

The experimental results regarding the chemical stability of the materials are shown in Fig. 5. This figure shows the evolution of OTC of the materials in pellet form along 160 oxidation-reduction cycles in the TGA apparatus at atmospheric pressure. The results show that the OTC reached values around  $0.15 \text{ mg O mg solid}^{-1}$  in the case of both pellets, and variations below 5% along cycling proved the stability of the new materials synthesized in the long term without agglomeration signs. Moreover the high Cu loads of these materials together with their high reactivity make them suitable candidates for the Ca/Cu looping process.

On the other hand, as it can be observed in Table 1, the Hg porosimetry analysis determined that the pellets supported onto  $Al_2O_3$  as well as  $MgAl_2O_4$  presented an increase in porosity in reduced forms with respect to the oxidized ones. In this way, the reduced pellets showed porosity values between 51 and 54% versus 43–48% obtained for the oxidized pellets. Therefore, a higher specific surface area was also found for the reduced pellets ( $21\text{--}24 \text{ m}^2 \text{ g}^{-1}$ ) versus the oxidized (around  $18 \text{ m}^2 \text{ g}^{-1}$ ). In general, the specific surface areas of powder and pellet materials presented similar values, however the porosity of the pellets has decreased a bit with respect to the materials in powder form. An important aspect to take into account is that this materials with high Cu loads have shown a significant increase in the values of porosity and BET surface area with regard to the other CuO-based materials with lower Cu loads that appear in the literature [27,29]. However, it was already reported that changes in the particle morphologies for Cu-based OCs do not influence the gas/solid reaction kinetics [50].

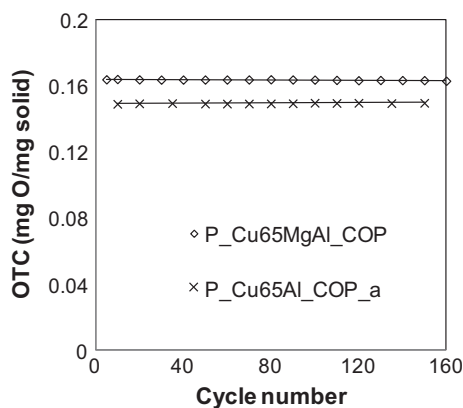


Fig. 5. Evaluation of the oxygen transport capacities for CuO-based pellets along 160 reduction-oxidation cycles.

### 3.2. Kinetic parameters

The kinetic study of the oxidation reaction of two different CuO-based materials, in powder and pellet form, was carried out in this work. Firstly, the kinetic parameters of the oxidation reaction of the CuO-based materials in powder form under atmospheric conditions were determined.

Fig. 6 shows the effect that reaction temperature has on powdered materials oxidation conversion at atmospheric pressure (in the range of 973 K to 1143 K) using a 10%vol O<sub>2</sub>. The conversion curves present a low dependence with temperature in agreement with the results obtained by other authors that analyzed the oxidation reaction of CuO-based materials with significantly lower CuO contents (between 10 and 20%wt CuO). An almost straight slope was also observed in these graphs which is typical of the evolution of conversion controlled by chemical reaction [26]. A very similar behavior has been observed in the oxidation conversion of the material supported onto MgAl<sub>2</sub>O<sub>4</sub>. The temperature had not a significant effect in the conversion curves and their slopes were practically straight, therefore a control by the chemical reaction could be in principle suitable to model the oxidation reaction.

A shrinking core model (SCM) that has been able to describe reduction [26,29,38,41] and oxidation [26,36,39,41] reactions of different metal compounds was applied in this work. From the straight slope of the curves it can be extracted that a plate-like geometry with the chemical reaction as the controlling step could be suitable to describe the conversion of the particles with time [26].

The general equation of a SCM controlled by chemical reaction for

any geometry can be expressed as [51]:

$$\frac{-1}{S_{\text{ext}}} \frac{N_A}{dt} = bk_s C_g^n \quad (4)$$

where  $N_A$  represents the number of moles of oxygen,  $S_{\text{ext}}$  is the surface area of the particles or pellet (m<sup>2</sup>),  $b$  is the stoichiometric coefficient of the oxidation reaction of the Cu,  $k_s$  is the reaction rate constant (mol<sup>1-n</sup> m<sup>3n-2</sup> s<sup>-1</sup> bar<sup>d</sup>),  $C_g$  is the gas concentration (mol m<sup>-3</sup>) and  $n$  is the reaction order.

Therefore this expression has been applied for plate-like geometry in the case of the material in powder form and cylindrical geometry for the pellet.

In the case of the material in powder form, the plate-like geometry according to the kinetic model under chemical reaction control can be expressed as [51]:

$$\frac{t}{\tau} = X_{\text{ox}} \quad (5)$$

where the time required for complete conversion has been calculated by the formula:

$$\tau = \frac{\rho_b L}{bk_s C_g^n} \quad (6)$$

where  $L$  represents the particle or pellet radius (m) and  $\rho_b$  represents the molar density of CuO in the particle (mol<sub>CuO</sub> m<sup>-3</sup>). and the reaction rate constant takes the following Arrhenius form:

$$k_s = k_0 \exp\left(\frac{-E_a}{RT}\right) \quad (7)$$

where  $k_0$  is the pre-exponential factor (mol<sup>1-n</sup> m<sup>3n-2</sup> s<sup>-1</sup> bar<sup>d</sup>),  $E_a$  represents the activation energy (J mol<sup>-1</sup>),  $R$  is the universal gas constant (J mol<sup>-1</sup> K<sup>-1</sup>) and  $T$  (K) is the reacting temperature that is used in the experiment.

Fig. 7 shows the experimental results (black lines) on the effect of the partial pressure of oxygen on particles conversion curves. It can be appreciated that complete conversion is quickly achieved (less than 100 s) for the entire range of the oxygen concentrations tested (5 vol% O<sub>2</sub>–40 vol% O<sub>2</sub>) and the slope of the curves remains practically straight for both materials. From the experimental data obtained with the materials in powder form, the kinetic parameters were determined using the preceding equations. The kinetic parameters are included in Table 2. The correlation coefficients obtained during the fitting of the experimental data with the SCM with chemical reaction control are also included in the table.

The reaction order has been determined from the slope of the representation of  $\ln(\rho_b L/b\tau)$  vs  $\ln(C_g)$ . The reaction order obtained for the oxidation reaction has been determined as 1 in the case of both

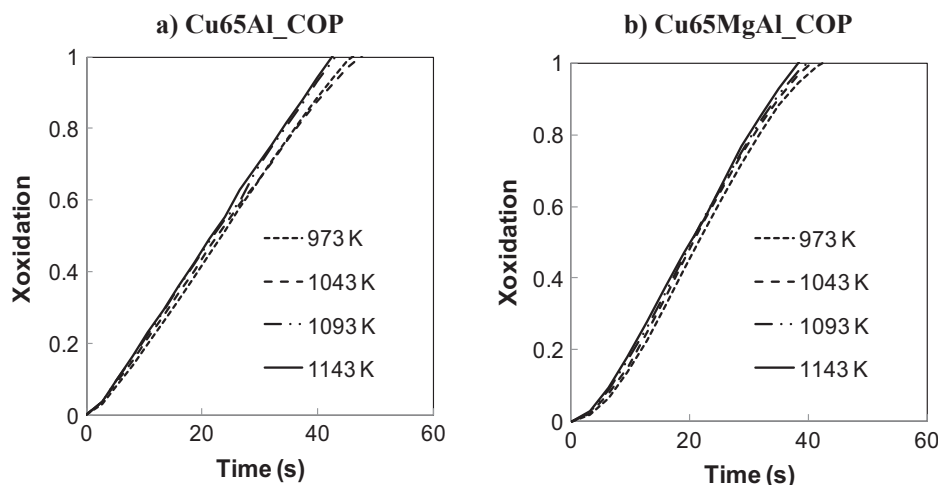


Fig. 6. Effect of temperature on oxidation conversion curves of the CuO-based powders obtained in the TGA apparatus (1 bar, 10%vol O<sub>2</sub>).

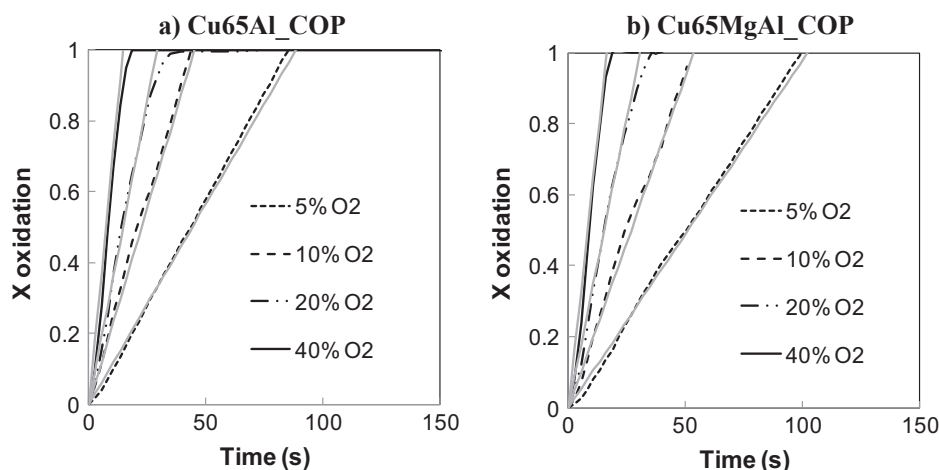


Fig. 7. Effect of gas concentration on oxidation conversion curves of CuO-based materials in powder and form obtained in the TGA apparatus (1 bar, 1123 K). Black lines are experimental results and grey lines represent theoretical results.

Table 2

Kinetic parameters determined for the oxidation reaction of both CuO-based materials.

Material form:	Cu65Al_COP Materials		Cu65MgAl_COP Materials	
	Powder	Pellet	Powder	Pellet
n	1 ( $R^2 = 0.9983$ )		1 ( $R^2 0.9978$ )	
$k_o$ , $\text{mol}^{1-n} \text{cm}^{3n-2} \text{s}^{-1} \text{bar}^d$	42 ( $R^2 0.9976$ )		40 ( $R^2 0.9996$ )	
$E_A$ , $\text{kJ mol}^{-1}$	$21.8 \pm 0.6$		$21.8 \pm 0.6$	
b	2		2	

P\_Cu65Al\_COP

a) Fully reduced

b) Partially oxidized

c) Fully oxidized

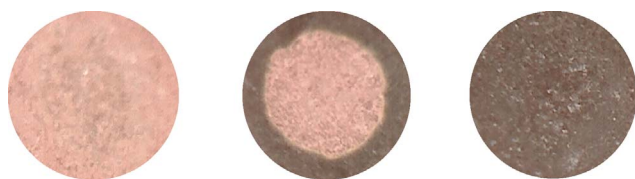


Fig. 8. Cross section photographs taken from the pellet P\_Cu65Al\_COP throughout different levels of the oxidation reaction.

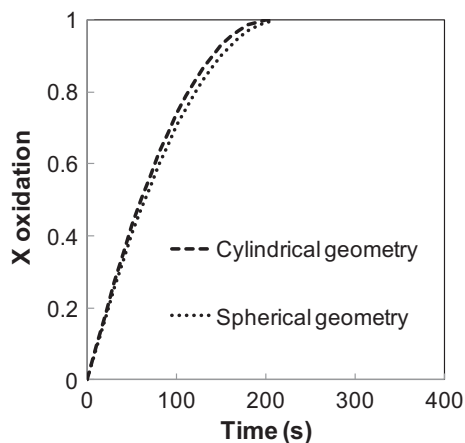


Fig. 9. Comparison between SCM model predictions (under chemical reaction control) when considering spherical and cylindrical geometry for the pellets P\_Cu65Al\_COP with 20%vol O<sub>2</sub> (1bar, 1123 K).

materials. These values are in agreement with those reported in the literature by other authors that tested the oxidation reaction of CuO-based materials with lower Cu contents [26,39]. On view of the

Table 3

Effective diffusivity and tortuosity values determined for the two pellets tested.

	P_Cu65Al_COP	P_Cu65MgAl_COP
$D_e$ ( $\text{m}^2 \text{s}^{-1}$ ) for O <sub>2</sub>	$1.24 \times 10^{-5}$	$5.09 \times 10^{-5}$
$\tau_{\text{pore}}$	1.14	1.10

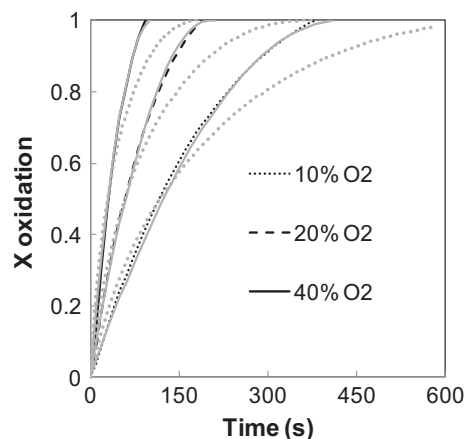


Fig. 10. Effect of gas concentration on oxidation conversion curves of CuO-based pellets predicted by the two models obtained in the TGA apparatus (1 bar, 1123 K). Black lines are experimental results, continuous grey lines represent theoretical results obtained by the SCM with CR control and discontinuous grey lines represent theoretical results obtained by the SCM that considers CR + DIF.

conversion curves represented in Fig. 7, the inert support nature had not an important effect on materials reactivity. The kinetic parameters  $k_o$  and  $E_a$  for each powdered material were determined using the effect of temperature in the reaction rates by the Arrhenius expression previously mentioned. In this way, in the representation of  $\ln(k_s)$  vs  $1/T$ , the term  $E_a/R$  is the slope of the representation and  $\ln(k_o)$  is defined by the ordinate. Low dependence of the reaction rate with temperature of

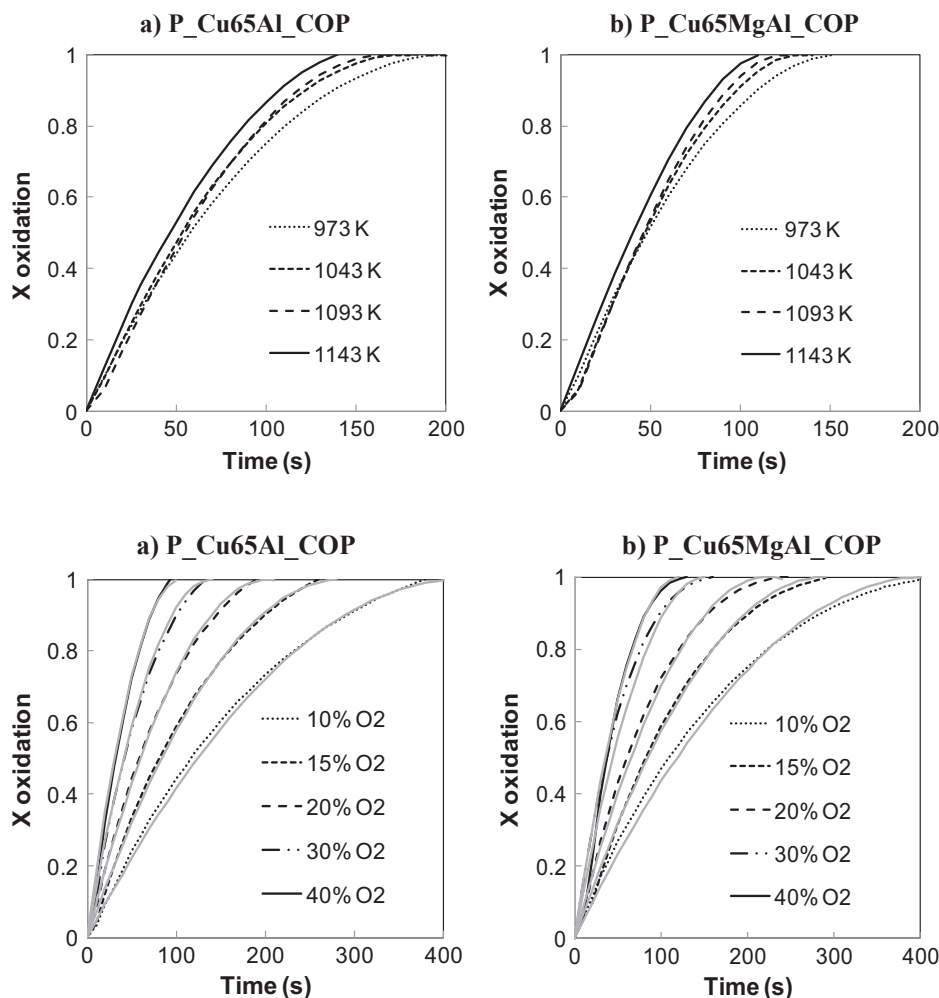


Fig. 11. Effect of temperature on oxidation conversion curves of CuO-based pellets obtained in the TGA apparatus (1 bar, 20%vol O<sub>2</sub>).

Fig. 12. Effect of gas concentration on oxidation conversion curves of CuO-based pellets obtained in the TGA apparatus (1 bar, 1123 K). Black lines are experimental results and grey lines represent theoretical results.

both materials has been observed in the range of temperatures tested with similar activation energy values of  $21.8 \pm 0.6 \text{ kJ mol}^{-1}$ . These values are also in agreement with those reported by other authors for the oxidation of CuO-based materials [26,39]. Once known the kinetic parameters of the oxidation reaction of powder materials they were included in the SCM with chemical reaction control. As it can be observed in Fig. 7, the experimental results (black lines) and model predictions (grey lines) fit pretty well using the SCM with kinetic control and plate-like geometry.

To adapt to the material requirements of the Ca/Cu looping process, that was designed to operate in fixed bed reactors, the materials were pelletized (see Table 1 for the main physical properties of the pelletized materials). In this way it is necessary to determine the reactivity, and find a suitable reaction model able to predict materials conversion. In order to give an insight about the reaction pattern followed by the CuO-based materials in pellet form, cross section photographs of the pellet particles were taken at different conversion levels. Fig. 8 shows photographs of transversal section of the pellet P\_Cu65Al\_COP\_a at different oxidation conversions. Fig. 8a shows a fully reduced pellet, Fig. 8b a partially oxidized pellet and, finally, Fig. 8c a fully oxidized pellet. It is observed that during the course of the oxidation reaction in the pellet, a clear external rim of oxidized material with a black color and an inner core of reddish reduced solid can be distinguished. Therefore, it seems that the reaction front moves towards the interior of the pellet and the interior of the particle does not react until the external layers are fully oxidized. It seems obvious that these results suggest that the material in pellet form follows a SCM that allows describing situations in which a clear front separates the solid reactant core from the external reacted

layer of the material.

In this way the SCM, first described by Yagi and Kunii [52] is proposed to fit the experimental data. According to this model (and to the pictures in Fig. 8), the oxidation of Cu to CuO would take place at a well defined inter-phase in the pellet particle. These could be physically justified by two situations: the chemical reaction is faster than diffusion of the O<sub>2</sub> to the interior of the pellet, and therefore as soon as the O<sub>2</sub> reaches the un-reacted front it is consumed by the Cu; or the diffusion of the O<sub>2</sub> through the external layer of oxide, that it is being formed, is the limiting step of the material conversion. In the case of the particles, it seems that the internal diffusion is not important during the course of the oxidation reactions, as it can be observed in the straight slopes obtained in Fig. 7, however in the case of the pellets this parameter could have an effect on the conversion. In this way, two different expressions for the SCM have been considered to describe the conversion of the pellets. In first place, it has been proposed that the chemical reaction controls the conversion of the pellet with cylindrical geometry [51], this is represented by Eq. (8).

$$\frac{t}{\tau} = 1 - (1 - X_{ox})^{1/2} \quad (8)$$

In second place, Hg porosimetry showed a slightly lower porosity of the oxidized pellets with respect to them in reduced form (see Table 1), therefore a second expression that considers the influence of the diffusion of the O<sub>2</sub> through the external oxide layer together with the chemical reaction has been considered (Eq. (9)).

Given the geometry of the pellets, (cylinders with a diameter equal to their height), and the similarity in the predictions of the model when



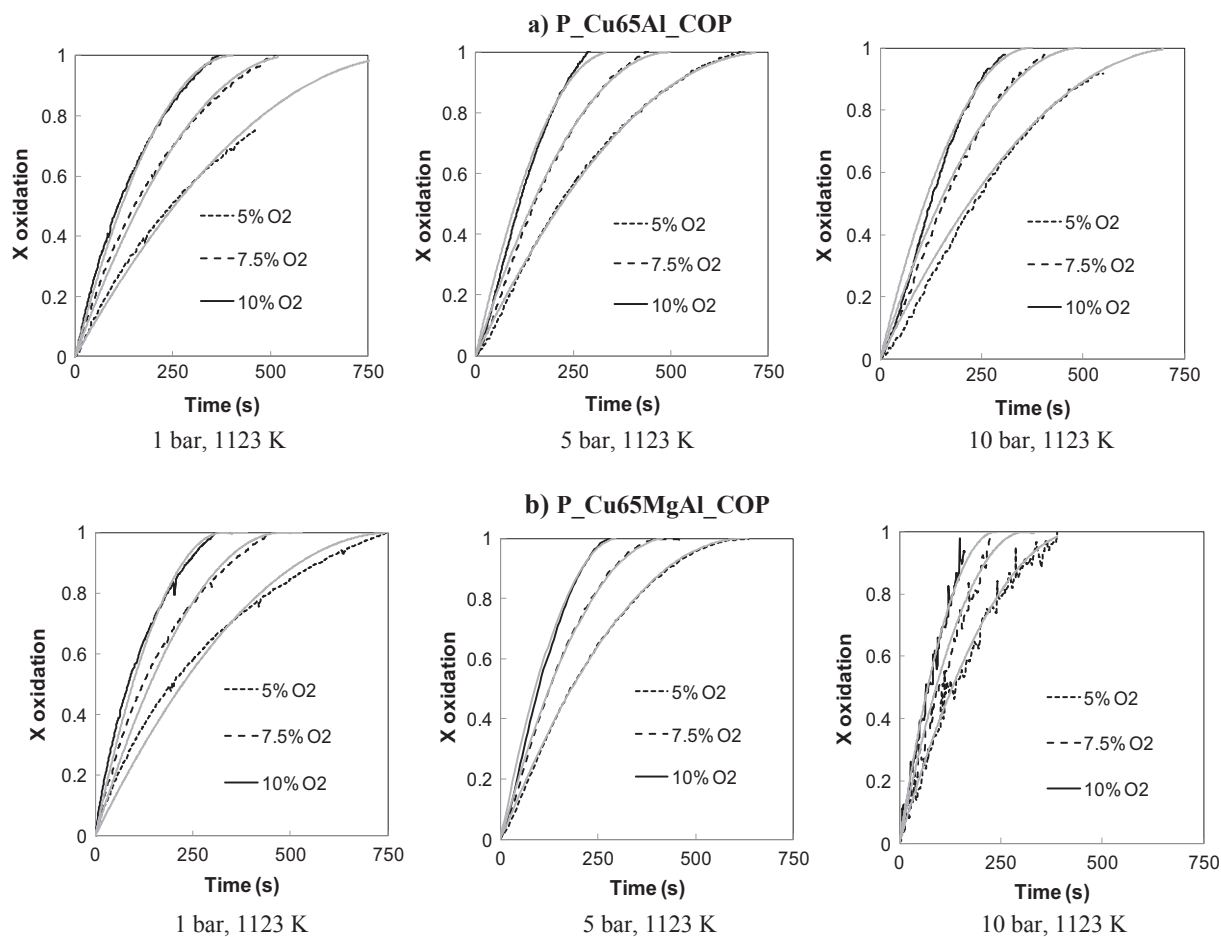


Fig. 13. Effect of pressure on oxidation conversion curves of CuO-based pellets obtained in the HPMSB apparatus (1123 K). Black lines are experimental results and grey lines represent theoretical results.

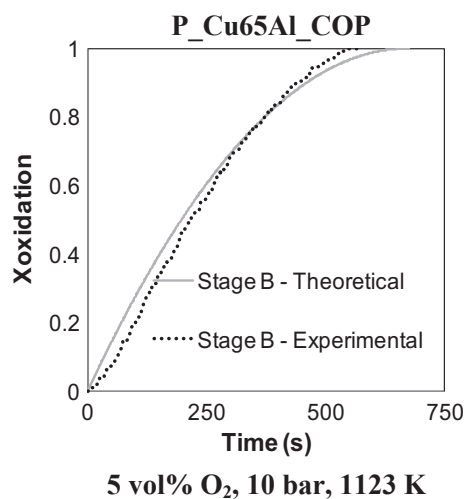


Fig. 14. Experimental and theoretical results of the prediction of the stage B of the Ca/Cu looping process with the P\_Cu65Al\_COP pellet in the HPMSB apparatus.

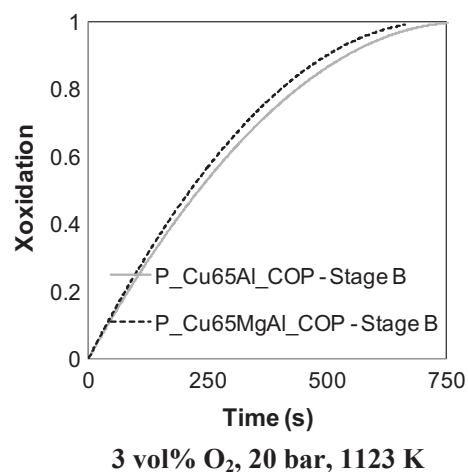


Fig. 15. Model predictions (considering chemical reaction control) of the stage B of the Ca/Cu looping process with both pellets.

considering spherical and cylindrical geometry (see Fig. 9), it was considered, for simplicity that the spherical geometry was also applicable for our symmetrical pellets.

In this way, the SCM that also considers the effect of internal diffusion through the solids has been applied taking into account the following assumptions: (a) the particle is spherical and its volume is constant; (b) mass and density of the particle are expected to vary

slightly as the reaction progresses; (c) the particle is isothermal; (d) the structure of the porous particle is uniform; (e) the porosity of the unreacted core is very small which means that the unreacted solid material is almost impervious to the reactant gases. The general equation of the model in terms of the change of the core radius ( $r_c$ ) at any time is described as follows [51]:

$$\frac{dr_c}{dt} = -\frac{bC_g}{\rho_b} \left[ \frac{r_c^2}{L^2 h_m} + \frac{(L-r_c)r_c}{RD_e} + \frac{1}{k_s C_g^{n-1}} \right] \quad (9)$$

The three terms that appear in the denominator of the Eq. (9) are related with the external mass-transfer, the internal (oxide-layer) diffusion and the chemical reaction rate, respectively. The parameter  $b$  is the stoichiometric coefficient,  $C_g$  is the molar concentration of the gas species,  $\rho_b$  is the molar density of the solid,  $L$  is the radius of the pellet,  $h_m$  represents the gas film mass transfer coefficient,  $D_e$  represents the effective diffusivity of the gas species  $i$  through the oxide layer,  $k_s$  is the reaction rate constant and  $n$  is the reaction order.

The first term in denominator in the Eq. (9) can be neglected, as no external mass transfer effects are avoided under the operating conditions in the TGA.

The reaction rate constant that takes part in the third term of the denominator of the global equation, has been considered that follows the Arrhenius form that appears in Eq. (7).

The effective diffusivity ( $D_e$ ) that appears in the second term of the equation can be calculated from gas diffusivity and the structural properties of the porous material using the formula:

$$D_e = \varepsilon \cdot \frac{D_{pore}}{\tau_{pore}} \quad (10)$$

where  $D_{pore}$  represents the mass diffusivity inside the mesopore,  $\varepsilon$  is the solid porosity and  $\tau_{pore}$  is the tortuosity of the pores. The tortuosity of the materials have been determined using the correlation between porosity-tortuosity proposed by Matyka et al. [53]:

$$\tau_{pore} = \sqrt{\frac{2\varepsilon}{3[1-1.09(1-\varepsilon)^{2/3}]} + \frac{1}{3}} \quad (11)$$

The gas diffusivity can be expressed as the combination of the bulk diffusivity ( $D_i$ ) and the Knudsen diffusivity ( $D_{Kn}$ ):

$$\frac{1}{D_{pore}} = \frac{1}{D_{Kn}} + \frac{1}{D_i} \quad (12)$$

The Knudsen diffusivity has been determined by the next equation, defined by:

$$D_{Kn} = \frac{d_{pore}}{3} \cdot \sqrt{\frac{8R \cdot T}{\pi M_i}} \quad (13)$$

where  $d_{pore}$  and  $M_i$  are expressed in meters and kg/mol, respectively.

The bulk diffusivity is calculated by the FGS (Fuller, Schettler and Giddings) correlation as follows [54]:

$$D_i = \frac{0.01013 \cdot T^{1.75} \sqrt{M_i^{-1} + M_k^{-1}}}{P(\frac{1}{\sqrt{v_i}} + \frac{1}{\sqrt{v_k}})^2} \quad (14)$$

where  $T$  and  $P$  are the operating temperature and pressure, respectively;  $M$  represents the molar weight of the gas specie ( $i = O_2$ ,  $k = N_2$ ) and  $v$  represents the diffusion volume for the each component ( $i = O_2$ ,  $k = N_2$ ).

In Table 3 the values obtained for the effective diffusivity and tortuosity of the different pellets are shown.

The effective diffusivity and the kinetic parameters determined with the SCM that only considers chemical reaction control for the oxidation reaction of the pellet have been included in the Eq. (9) at 1123 K and each specific partial pressure of gas. In this way, the parameter  $r_c$  is the only unknown parameter in Eq. (9) and the evolution of  $r_c$  as function of time can be evaluated. The differential equation taking into account internal diffusion and chemical reaction terms for each specific material and conditions has been solved using the Runge-Kutta fourth-order method (RK4) programmed in Visual Basic. The theoretical results predicted using this model (discontinuous grey lines) are shown in Fig. 10 in contrast with the theoretical results predicted using the SCM with chemical reaction control (continuous grey lines) for the pellet supported onto  $Al_2O_3$ . The theoretical results obtained by the SCM with

chemical reaction (CR) control are very similar to the experimental results, however the theoretical results obtained with the SCM that also considers internal diffusion (DIF) are not so close to the experimental ones. Then, it seem obvious that the oxidation reaction of highly loaded CuO-based materials, both in particles and pellet form, is kinetically controlled. Therefore, this model will be applied for fitting the experimental oxidation conversion data obtained for the different solids.

Fig. 11 shows the effect of temperature from 973 K to 1143 K on the conversion of the pellets with 20 vol%  $O_2$ . The oxidation reaction was fast achieving complete conversion of both pellets in less than 200 s. In the same way as for powdered materials, the oxidation with  $O_2$  presented a low dependence with temperature and the slope of the oxidation curves at different temperatures was practically constant which seems to indicate that the diffusion resistance is not important during the oxidation reaction of these solids even at lower temperatures.

To prove the intrinsic character of the kinetic parameters calculated for powdered materials, they were included in the Eq. (8) of the model that considers cylindrical geometry and that has been applied to describe the evolution of the pellet oxidation conversion. Fig. 12 shows the experimental results (black lines) and model predictions (grey lines) on the effect of the partial pressure of oxygen on pellet conversion curves at 1123 K. The theoretical curves obtained by the model show that the experimental results fit pretty well applying the SCM with chemical reaction control for the oxidation reaction of the pellets with 20%vol  $O_2$ , 1 bar and 1123 K were respectively 0.9982 for the P\_Cu65Al\_COP and 0.9975 for the P\_Cu65MgAl\_COP. Therefore it seems that the model is suitable to fit the oxidation reaction of this kind of materials as correlation factors very close to 1 have been obtained.

Therefore the evolution of materials oxidation conversion in powder and pellet form was successfully described with a SCM with kinetic regime, being able to use the same kinetic parameters for particles and pellets and considering that the geometry of the material is the only difference to be taken into account in the model.

### 3.3. Effect of total pressure

To analyze the effect of total pressure on the behavior of the CuO-based materials, experiments at a fixed temperature (1123 K) and in a narrow range of  $O_2$  concentrations (from 5 vol%  $O_2$  to 10 vol%  $O_2$ ) were carried out at the HPMSB for the pellet P\_Cu65Al\_COP varying the total pressure in the apparatus for 1, 5 and 10 bar in each experimental campaign. As it has been previously mentioned, a similar space velocity for the gas was used in the HPMSB in order to compare the experimental results at atmospheric and pressurized conditions.

First, the kinetic parameters obtained from powders in the TGA at atmospheric pressure were used to fit the experimental data obtained for the materials in the HPMSB at 1 bar. The results demonstrated that the kinetic parameters obtained from powders at the TGA adjusted fairly well with the experimental data obtained for pellets in the HPMSB which indicates that no effects of gas dispersion or diffusion are involved in the HPMSB.

Fig. 13 represents the oxidation conversion curves for the pellets tested at 1123 K and three different pressures. As it can be observed the pellet supported onto  $Al_2O_3$  was barely affected by pressure, being a bit faster the reaction rate of the oxidation reaction at higher pressures as it could be expected. In the case of the pellet supported onto to  $MgAl_2O_4$ , the increase in total pressure in the system broke the pellet increasing the contact surface area of the material and helping the reaction to progress faster.

An apparent pre-exponential factor was determined as a function of total pressure ( $k_{0,P}$ ) and the pre-exponential factor obtained at atmospheric pressure ( $k_0$ ) using the following expression:

$$K_{0,P} = k_0 \cdot P^d \quad (15)$$

The values obtained for parameter  $d$  are very low, varying from 0.08 for the pellet supported on to  $\text{Al}_2\text{O}_3$  to 0.12 for the pellet supported on to  $\text{MgAl}_2\text{O}_4$ , which means that the total pressure on the system practically has not affected the reactivity of the materials. The pellet supported onto  $\text{MgAl}_2\text{O}_4$ , which does not contain any binder, is less compacted and the increase of pressure makes that the pellet cannot endure without fracturing. Therefore, it seems that if some agglutinant is incorporated to the pellet, this should present a high mechanical stability under pressurizing conditions like the pellet supported on to  $\text{Al}_2\text{O}_3$  and similar reactivity than the pellet tested under atmospheric conditions.

As well as in the tests at atmospheric pressure, the theoretical results (grey lines) obtained by the SCM with control of chemical reaction fit fairly well with the experimental results (black lines) obtained in the HPMSB at 5 bar and 10 bar (Fig. 13).

The stage B of the process has been proposed to be performed under pressure to reduce the sorbent calcination in this step, and with diluted air to avoid any hot spot in the reactor. According with the works that appear in the literature related with the Ca/Cu process design [17,22], the operation in a pressure range between 10 and 20 bars and  $\text{O}_2$  concentrations between 3 and 5%vol is a suitable window for the process. Therefore, in Figs. 14 and 15 the evolution of the pellet conversion under two different possible operation conditions for the step B has been explored. In this way, Fig. 14 shows the experimental and theoretical results of the oxidation conversion of the pellet P\_Cu65Al\_COP obtained under one typical conditions of the step B (5 vol%  $\text{O}_2$ , 1123 K, 10 bar). As it can be appreciated from the figure, it is possible to predict the evolution of conversion of the pellet by the SCM with chemical reaction control using the kinetic parameters obtained at atmospheric pressure and applying the factor  $d$  in the pre-exponential factor correlation.

On the other hand, the model predictions of the oxidation conversion of both pellets (applying the SCM with chemical reaction control) considering other possible conditions for the step B (3%vol  $\text{O}_2$ , 1123 K and 20 bar) have been plotted in Fig. 15. As it can be noted, both pellets should present a quite similar behavior during the oxidation reaction without important influence of total pressure in the system as well as the material used as support. The mentioned results suggested that the pressure has not an important effect on the oxidation kinetics of high loaded CuO-based materials and these results are in agreement with a recent publication [47] in which the authors analyzed the reduction reaction of  $\text{CuO}/\text{Al}_2\text{O}_3$  particles and did not find changes on the evolution of the reduction conversion with the increase of the pressure in the system. Therefore, the development of the kinetic behavior of these materials under pressurized conditions will provide a better knowledge of the behavior of the CuO-based pellets during the operation of the step B at the fixed bed reactor during the startup of the Ca/Cu looping process since, in view of these results, the oxidation reaction of the Cu material in this step should not strongly affected by pressure.

#### 4. Conclusions

The oxidation reaction of two CuO-based materials with high Cu loads was studied at atmospheric and pressurized conditions. The materials in powder and pellet form presented a low dependence with temperature in the range of temperatures tested (973 K–1143 K). The straight slope of the oxidation curves of the particles at different partial pressures of oxygen suggested that the evolution of the conversion was kinetically controlled. Moreover, it was observed that the material used as support ( $\text{Al}_2\text{O}_3$  or  $\text{MgAl}_2\text{O}_4$ ) had not a significant influence on materials reactivity. Cross-section photographs taken during the course of oxidation reaction of one single pellet suggested that the SCM could be applied appropriately to study the oxidation reaction. The kinetic parameters obtained for the materials in powder form were used to fit the experimental data obtained for the pellets. The evolution of the Cu oxidation of particles and pellets was successfully modeled by the SCM with chemical reaction control but adapted to plate-like geometry for

powders and cylindrical geometry for pellets. On the other hand, it was found that the total pressure of the system had not an important effect on kinetics and the same kinetic parameters obtained under atmospheric conditions can be suitable to simulate the oxidation conversion under pressurized conditions.

#### Acknowledgements

This work acknowledges the support by European Union Seventh Frame Programme FP7 under grant agreement n° 608512 (ASCENT Project). Laura Díez-Martín acknowledges the FPI fellowship (ENE 2012-37936-CO2-01, BES-2013-064616 financed by MINECO).

#### References

- [1] IPCC. Mitigation of Climate Change. Contribution of Working Group III to the Fifth Assessment Report of the Intergovernmental Panel on Climate Change. Cambridge University Press, Cambridge, United Kingdom and New York, NY, USA; 2014.
- [2] Meerman JC, Hamborg ES, van Keulen T, Ramírez A, Turkenburg WC, Faaij APC. Techno-economic assessment of  $\text{CO}_2$  capture at steam methane reforming facilities using commercially available technology. *Int J Greenhouse Gas Control* 2012;9:160–71.
- [3] Rostrup-Nielsen JR, Sehested J, Nørskov JK. Hydrogen and synthesis gas by steam- and  $\text{CO}_2$  reforming. *Adv Catal* 2002;47:65–139.
- [4] Damen K, Troost Mv, Faaij A, Turkenburg W. A comparison of electricity and hydrogen production systems with  $\text{CO}_2$  capture and storage. Part A: review and selection of promising conversion and capture technologies. *Prog Energy Combust Sci* 2006;32(2):215–46.
- [5] Kumar A, Baldea M, Edgar TF, Ezekoye OA. Smart manufacturing approach for efficient operation of industrial steam-methane reformers. *Ind Eng Chem Res* 2015;54(16):4360–70.
- [6] Sircar S, Golden TC. Purification of hydrogen by pressure swing adsorption. *Sep Sci Technol* 2000;35(5):667–87.
- [7] Boot-Handford ME, Abanades JC, Anthony EJ, Blunt MJ, Brandani S, Mac Dowell N, et al. Carbon capture and storage update. *Energy Environ Sci* 2014;7(1):130–89.
- [8] Balasubramanian B, Lopez Ortiz A, Kaytakoglu S, Harrison DP. Hydrogen from methane in a single-step process. *Chem Eng Sci* 1999;54(15):3543–52.
- [9] Harrison DP. Sorption-enhanced hydrogen production: a review. *Ind Eng Chem Res* 2008;47(17):6486–501.
- [10] Lee DK, Baek IH, Yoon WL. Modeling and simulation for the methane steam reforming enhanced by in situ  $\text{CO}_2$  removal utilizing the CaO carbonation for  $\text{H}_2$  production. *Chem Eng Sci* 2004;59(4):931–42.
- [11] Lopez Ortiz A, Harrison DP. Hydrogen production using sorption-enhanced reaction. *Ind Eng Chem Res* 2001;40(23):5102–9.
- [12] Martavaltzi CS, Lemonidou AA. Hydrogen production via sorption enhanced reforming of methane: development of a novel hybrid material—reforming catalyst and  $\text{CO}_2$  sorbent. *Chem Eng Sci* 2010;65(14):4134–40.
- [13] Ramkumar S, Fan L-S. Calcium looping process (CLP) for enhanced noncatalytic hydrogen production with integrated carbon dioxide capture. *Energy Fuels* 2010;24(8):4408–18.
- [14] Yi KB, Harrison DP. Low-pressure sorption-enhanced hydrogen production. *Ind Eng Chem Res* 2005;44(6):1665–9.
- [15] Yoon YI, Baek IH, Park SD. Enhancement of  $\text{H}_2$  production by combination with  $\text{CO}_2$  absorption in steam methane reforming in bench scale. *J Ind Eng Chem* 2007;13(5):842–9.
- [16] Abanades JC, Murillo R, Fernandez JR, Grasa G, Martínez I. New  $\text{CO}_2$  capture process for hydrogen production combining Ca and Cu chemical loops. *Environ Sci Technol* 2010;44(17):6901–4.
- [17] Fernández JR, Abanades JC, Murillo R, Grasa G. Conceptual design of a hydrogen production process from natural gas with  $\text{CO}_2$  capture using a Ca–Cu chemical loop. *Int J Greenhouse Gas Control* 2012;6:126–41.
- [18] Martini M, Martínez I, Romano MC, Chiesa P, Gallucci F, van Sint Annaland M. Increasing the carbon capture efficiency of the Ca/Cu looping process for power production with advanced process schemes. *Chem Eng J* 2017;328:304–19.
- [19] Martini M, van den Berg A, Gallucci F, van Sint Annaland M. Investigation of the process operability windows for Ca–Cu looping for hydrogen production with  $\text{CO}_2$  capture. *Chem Eng J* 2016;303:73–88.
- [20] Abanades JC, Murillo R. Method for recovering  $\text{CO}_2$  by means of CaO and the exothermic reduction of a solid, Patent EP09382169; 2009.
- [21] Grasa G, Navarro MV, López JM, Díez-Martín L, Fernández JR, Murillo R. Validation of the  $\text{H}_2$  production stage via SER under relevant conditions for the Ca/Cu reforming process practical application. *Chem Eng J* 2017;324:266–78.
- [22] Fernández JR, Abanades JC, Murillo R. Modeling of Cu oxidation in adiabatic fixed-bed reactor with  $\text{N}_2$  recycling in a Ca/Cu chemical loop. *Chem Eng J* 2013;232:442–52.
- [23] Alarcón JM, Fernández JR.  $\text{CaCO}_3$  calcination by the simultaneous reduction of CuO in a Ca/Cu chemical looping process. *Chem Eng Sci* 2015;137:254–67.
- [24] Alarcón JM, Fernández JR, Abanades JC. Study of a Cu–CuO chemical loop for the calcination of  $\text{CaCO}_3$  in a fixed bed reactor. *Chem Eng J* 2017;325(Supplement C):208–20.
- [25] Adanez J, Abad A, García-Labiano F, Gayán P, de Diego LF. Progress in chemical-

- looping combustion and reforming technologies. *Prog Energy Combust Sci* 2012;38(2):215–82.
- [26] Adánez J, de Diego LF, García-Labiano F, Gayán P, Abad A, Palacios JM. Selection of oxygen carriers for chemical-looping combustion. *Energy Fuels* 2004;18(2):371–7.
- [27] Arjmand M, Azad A-M, Leion H, Lyngfelt A, Mattisson T. Prospects of  $\text{Al}_2\text{O}_3$  and  $\text{MgAl}_2\text{O}_4$ -supported CuO oxygen carriers in chemical-looping combustion (CLC) and chemical-looping with oxygen uncoupling (CLOU). *Energy Fuels* 2011;25(11):5493–502.
- [28] Chuang SY, Dennis JS, Hayhurst AN, Scott SA. Development and performance of Cu-based oxygen carriers for chemical-looping combustion. *Combust Flame* 2008;154(1–2):109–21.
- [29] García-Lario AL, Martínez I, Murillo R, Grasa G, Fernández JR, Abanades JC. Reduction kinetics of a high load Cu-based pellet suitable for Ca/Cu chemical loops. *Ind Eng Chem Res* 2013;52(4):1481–90.
- [30] Gayán P, Adánez-Rubio I, Abad A, de Diego LF, García-Labiano F, Adánez J. Development of Cu-based oxygen carriers for chemical-looping with oxygen uncoupling (CLOU) process. *Fuel* 2012;96:226–38.
- [31] Gayán P, Forero CR, Abad A, de Diego LF, García-Labiano F, Adánez J. Effect of support on the behavior of Cu-based oxygen carriers during long-term CLC Operation at temperatures above 1073 K. *Energy Fuels* 2011;25(3):1316–26.
- [32] Imtiaz Q, Kierzkowska AM, Broda M, Müller CR. Synthesis of Cu-rich,  $\text{Al}_2\text{O}_3$ -stabilized oxygen carriers using a coprecipitation technique: redox and carbon formation characteristics. *Environ Sci Technol* 2012;46(6):3561–6.
- [33] Mattisson T, Järnäs A, Lyngfelt A. Reactivity of some metal oxides supported on alumina with alternating methane and oxygen application for chemical-looping combustion. *Energy Fuels* 2003;17(3):643–51.
- [34] Roux S, Bensakhria A, Antonini G. Study and improvement of the regeneration of metallic oxides used as oxygen carriers for a new combustion process. *Int J Chem Reactor Eng* 2006;4.
- [35] Rydén M, Jing D, Källén M, Leion H, Lyngfelt A, Mattisson T. CuO-Based oxygen-carrier particles for chemical-looping with oxygen uncoupling – experiments in batch reactor and in continuous operation. *Ind Eng Chem Res* 2014;53(15):6255–67.
- [36] Chuang SY, Dennis JS, Hayhurst AN, Scott SA. Kinetics of oxidation of a reduced form of the Cu-based oxygen-carrier for use in chemical-looping combustion. In: Yue G, Zhang H, Zhao C, Luo Z, editors. *Proceedings of the 20th international conference on fluidized bed combustion*. Berlin, Heidelberg: Springer, Berlin Heidelberg; 2010. p. 512–8.
- [37] Ishida M, Jin H, Okamoto T. Kinetic behavior of solid particle in chemical-looping combustion: suppressing carbon deposition in reduction. *Energy Fuels* 1998;12(2):223–9.
- [38] Liu X, Song F, Wen Z. A novel dimensionless form of unreacted shrinking core model for solid conversion during chemical looping combustion. *Fuel* 2014;129:231–7.
- [39] Maya JC, Chejne F. Modeling of oxidation and reduction of a copper-based oxygen carrier. *Energy Fuels* 2014;28(8):5434–44.
- [40] Noorman S, Gallucci F, van Sint Annaland M, Kuipers JAM. A theoretical investigation of CLC in packed beds. Part 2: Reactor model. *Chem Eng J* 2011;167(1):369–76.
- [41] Ortiz M, Gallucci F, Melchiori T, Spallina V, van Sint Annaland M. Kinetics of the reactions prevailing during packed-bed chemical looping combustion of syngas using ilmenite. *Energy Technology* 2016;4(10):1137–46.
- [42] Abad Secades A, Adánez Elorza J, Diego Poza LFd, García Labiano F, Gayán Sanz P. Effect of pressure on the behavior of copper-, iron-, and nickel-based oxygen carriers for chemical-looping combustion. *Energy Fuels* 2006;20(1):26–33.
- [43] Szekely J, Evans JW. A structural model for gas–solid reactions with a moving boundary. *Chem Eng Sci* 1970;25(6):1091–107.
- [44] Go KS, Son SR, Kim SD. Reaction kinetics of reduction and oxidation of metal oxides for hydrogen production. *Int J Hydrogen Energy* 2008;33(21):5986–95.
- [45] Hossain MM, de Lasa HL. Reactivity and stability of Co-Ni/ $\text{Al}_2\text{O}_3$  oxygen carrier in multicycle CLC. *AIChE J* 2007;53(7):1817–29.
- [46] Hamers HP, Gallucci F, Williams G, Cobden PD, van Sint Annaland M. Reactivity of oxygen carriers for chemical-looping combustion in packed bed reactors under pressurized conditions. *Energy Fuels* 2015;29(4):2656–63.
- [47] San Pio MA, Gallucci F, Roghair I, van Sint Annaland M. Gas-solids kinetics of CuO/ $\text{Al}_2\text{O}_3$  as an oxygen carrier for high-pressure chemical looping processes: the influence of the total pressure. *Int J Hydrogen Energy* 2017;42(17):12111–21.
- [48] Hu C-Y, Shih K, Leckie JO. Formation of copper aluminate spinel and cuprous aluminate delafossite to thermally stabilize simulated copper-laden sludge. *J Hazard Mater* 2010;181(1):399–404.
- [49] Abad Secades A, Adánez Elorza J, Corbella BM, Diego Poza LFd, García Labiano F, Gayán Sanz P, et al. Development of Cu-based oxygen carriers for chemical-looping combustion. *Fuel* 2004;1757:1749–57.
- [50] San Pio MA, Roghair I, Gallucci F, van Sint Annaland M. Investigation on the decrease in the reduction rate of oxygen carriers for chemical looping combustion. *Powder Technol* 2016;301:429–39.
- [51] Levenspiel O. *Chemical reactor engineering*. 3rd ed. Wiley; 1998.
- [52] Yagi S, Kunii D. Studies on combustion of carbon particles in flames and fluidized beds. *Symp (Int) Combust* 1955;5(1):231–44.
- [53] M. Matyka, Z. Koza, *How to Calculate Tortuosity Easily?*; 2012.
- [54] Fuller EN, Schettler PD, Giddings JC. New method for prediction of binary gas-phase diffusion coefficients. *Ind Eng Chem* 1966;58(5):18–27.